HHS Public Access

Author manuscript

Cell Metab. Author manuscript; available in PMC 2021 October 12.

Published in final edited form as:

Cell Metab. 2020 September 01; 32(3): 447–456.e6. doi:10.1016/j.cmet.2020.08.004.

Alpha-Ketoglutarate, an Endogenous Metabolite, Extends Lifespan and Compresses Morbidity in Aging Mice

Azar Asadi Shahmirzadi[1,2], **Daniel Edgar**[1], **Chen-Yu Liao**[1], **Yueh-Mei Hsu**[1], **Mark Lucanic**[1], **Arash Asadi Shahmirzadi**[1], **Christopher D. Wiley**[1], **Garbo Gan**[1], **Dong Eun Kim**[1], **Herbert G. Kasler**[1], **Chisaka Kuehnemann**[1], **Brian Kaplowitz**[1], **Dipa Bhaumik**[1], **Rebeccah R. Riley**[1], **Brian K. Kennedy**[1,3,4,5,6,*], **Gordon J. Lithgow**[1,2,*]

[1]The Buck Institute for Research on Aging, 8001 Redwood Blvd., Novato, CA 94945, USA

[2]USC Leonard Davis School of Gerontology, University of Southern California, 3715 McClintock Ave., Los Angeles, CA 90191, USA

[3]Healthy Longevity Programme, Yong Loo Lin School of Medicine, National University of Singapore, 10 Medical Dr., Singapore 117597, Singapore

[4]Centre for Healthy Longevity, National University Health System, Singapore, 1E Kent Ridge Rd., Singapore 119228, Singapore

[5]Singapore Institute of Clinical Sciences, A*STAR, Singapore 117609, Singapore

[6]Lead Contact

SUMMARY

Metabolism and aging are tightly connected. Alpha-ketoglutarate is a key metabolite in the tricarboxylic acid (TCA) cycle, and its levels change upon fasting, exercise, and aging. Here, we investigate the effect of alpha-ketoglutarate (delivered in the form of a calcium salt, CaAKG) on healthspan and lifespan in C57BL/6 mice. To probe the relationship between healthspan and lifespan extension in mammals, we performed a series of longitudinal, clinically relevant measurements. We find that CaAKG promotes a longer, healthier life associated with a decrease in levels of systemic inflammatory cytokines. We propose that induction of IL-10 by dietary AKG suppresses chronic inflammation, leading to health benefits. By simultaneously reducing

*Correspondence: bkennedy@nus.edu.sg (B.K.K.), glithgow@buckinstitute.org (G.J.L.).

AUTHOR CONTRIBUTIONS

G.J.L. and B.K.K. supervised the study. D.E., Azar Asadi Shahmirzadi, G.J.L., and B.K.K. designed experiments. Azar Asadi Shahmirzadi, D.E., C.-Y.L., Y.-M.H., and G.G. investigated the healthspan data. Azar Asadi Shahmirzadi and Arash Asadi Shahmirzadi undertook the formal analysis. C.-Y.L., R.R.R., Y.-M.H., G.G., and Azar Asadi Shahmirzadi investigated the mouse samples. B.K. performed the metabolic studies. Azar Asadi Shahmirzadi and H.G.K. investigated the immune phenotype with H.G.K. undertaking the flow cytometric assays. C.D.W. and C.K. provided primers and C.D.W. helped with senescent-related experiments. D.E.K. and Azar Asadi Shahmirzadi performed the hair follicle melanocyte experiments. Azar Asadi Shahmirzadi, B.K.K., and G.J.L. wrote the paper with input from all authors.

DECLARATION OF INTERESTS

G.J.L. and M.L. are co-founders of Gerostate Alpha, a company aimed at developing drugs for aging, and are shareholders in Ponce de Leon Health. D.E. and Azar Asadi Shahmirzadi are shareholders in Ponece de Leon Health. B.K.K. is a board member and equity holder at Ponce de Leon Health. G.J.L., B.K., M.L., D.E., and Azar Asadi Shahmirzadi are named inventors on a preliminary patent application related to this discovery.

SUPPLEMENTAL INFORMATION

Supplemental Information can be found online at https://doi.org/10.1016/j.cmet.2020.08.004.

frailty and enhancing longevity, AKG, at least in the murine model, results in a compression of morbidity.

Graphical Abstract

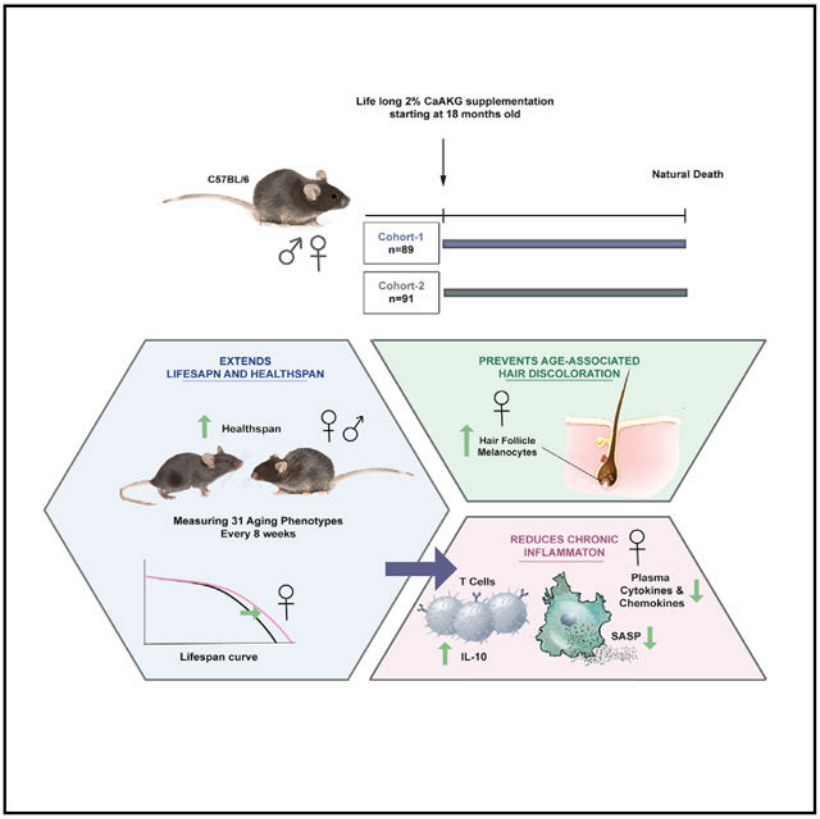

In Brief

Asadi Shahmirzadi et al. report that an alpha-ketoglutarate-supplemented diet extends lifespan of middle-aged female mice and increases healthspan in both sexes. With simultaneous reduction in frailty and increase in longevity, the intervention compresses morbidity. AKG suppresses chronic inflammation and induces secretion of IL-10 in T cells of female mice.

INTRODUCTION

The decline in early life mortality since the 1950s has resulted in a dramatic demographic shift toward an aged population. Aging manifests as a decline in health, multiple organ dysfunction, increased vulnerability to chronic disease, and degraded quality of life. A variety of genetic and pharmacological interventions, identified mainly in non-vertebrate model organisms, extend lifespan (Friedman and Johnson, 1988; Harrison et al., 2009; Kenyon et al., 1993; Wood et al., 2004), but the relationship to healthspan, the disease-free and functional period of life, is unclear (Bansal et al., 2015; Hahm et al., 2015; Hansen and Kennedy, 2016).

The frailty concept was initially developed to quantify human vulnerability to adverse health outcomes (Fried et al., 2001). However, corresponding comprehensive indices in mice were seldom applied to aging studies (Whitehead et al., 2014). Recently, there is increasing awareness that frailty might be a critical tool to measure healthspan in longevity studies (Kane et al., 2016; Rockwood et al., 2017). To study health during an aging intervention, we performed a series of longitudinal, clinically relevant healthspan measurements utilizing the frailty index developed by Howlett and colleagues (Whitehead et al., 2014).

Here, we show that alpha-ketoglutarate (delivered in the form of a calcium salt, CaAKG), a key metabolite in the tricarboxylic acid (TCA) cycle that is reported to extend lifespan in both *C. elegans* (Chin et al., 2014) and *Drosophila* (Su et al., 2019), can significantly extend lifespan and healthspan in mice. AKG is involved in various fundamental processes, including central metabolism, collagen synthesis (Myllyharju, 2003), epigenetic regulation (Tsukada et al., 2006), and stem cell proliferation (TeSlaa et al., 2016). Due to its broad biological roles, AKG has been a subject of interest for researchers in various fields (Zdzisińska et al., 2017). We find that CaAKG supplementation promotes longer, healthier life associated with decreased levels of inflammatory cytokines in mice.

RESULTS

C57BL/6 mice were fed regular chow and then switched to a diet containing CaAKG at 540 days of age (Figure S1). We assessed two independent cohorts of mice, each consisting of 45 ± 2 females and 45 ± 2 males (total of 182 animals), allowing us to assess reproducibility for longevity effects of CaAKG. Dietary-supplemented 2% CaAKG (w/w) increases survival in both cohorts of female mice (Figures 1A and 1B). In the first cohort of females, median lifespan and survival (age at 90^{th} percentile mortality) were significantly extended by 16.6% and 19.7% from inception of CaAKG feeding. In the second cohort of mice, lifespan and survival were significantly extended by 10.5% and 8% (Figures 1A and 1B; Table S1). Although improved survival for males was not significant in either cohort (Figures 1D and 1E), median lifespan was extended for 9.6% and 12.8% from inception of treatment (Table S1).

To assess healthspan, we applied measurements based on a clinically relevant frailty index (Parks et al., 2012; Whitehead et al., 2014), which consists of 31 phenotypes that are indicators of age-associated health deterioration with each phenotype scored in a blinded manner on a 0, 0.5, or 1 scale, based on severity (Figure S1). Measurements were repeated approximately every 8 weeks, providing eight and seven sets of data, respectively, for male and female groups. A baseline health assessment was assessed at the start of treatment at 18 months. The total frailty score, which is the average of 31 frailty phenotypes, was calculated for each animal at every time point (Figures 2A–2F) and indicates the state of increased vulnerability to adverse health outcomes, comparable to morbidity.

Since our experimental design takes repeated-measurements on the same mice over time, our analysis took into account the probability that measurements for a given mouse will be correlated. We applied mixed models to analyze our longitudinal data (Figures 2A and 2B). In the current mixed model, every mouse with a unique ID was treated as a random effect.

Treatment and time were treated as fixed effects (Wu, 2010). Further, the chi-square statistic was calculated for comparing the fit of the current mixed model to a simpler ANOVA, which does not account for repeated measures. The very small p value ($p < 0.0001$) for chi-square indicates that our current analysis model is very efficient. Our results show that, in both female and male animals, CaAKG decreases incidence and severity of aging phenotypes and postpones morbidity (Figures 2A and 2B).

Since the age for onset of age-related phenotypes can be quite heterogeneous in mammals, we plotted frailty not only as a function of chronological time, but also in proportion to the lifespan of each mouse by binning scores within ten percentiles (Figures 2C and 2D). This allowed us to align assessments with respect to biologic age. Our findings show that CaAKG treatment decreases the proportion of life in which the animal is frail and vulnerable to adverse health incomes (determined as the area under the frailty curve and calculated at a 46% reduction for females and 41% for males; Figures 2C and 2D). This improvement in healthy days of life is larger than the increase in lifespan. Through this extensive frailty data analysis, we have demonstrated that dietary CaAKG supplementation results in morbidity compression.

To determine whether there is a correlation between the frailty index and life expectancy, we plotted the total score of each animal in a given time point against its remaining days of life. We applied repeated-measures correlation (rmcorr) to analyze our longitudinal data (Bland and Altman, 1995). rmcorr accounts for dependence of the dataset and evaluates the overall common intra-individual association between measurements (Bakdash and Marusich, 2017). Our data show that higher scores for mice correlates negatively with life expectancy and can be considered as a risk factor (Figures 2E and 2F). These are analogous to studies in humans whereby frailty is a property of age, but not all individuals acquire frailty to the same extent. Thus, frailty score predicts mortality significantly but imperfectly.

The result of rmcorr indicates that absolute value of slope corresponding to the AKG treatment cohort is smaller than the one for the control cohort. To further prove that there is a statistically meaningful difference between these two slopes, we applied a mixed model to the combined dataset of AKG and control cohorts. In the current model, we treated remaining life and treatment as fixed factors and each mouse as a random factor. We found that AKG treatment significantly decreases the magnitude of the regression slopes in both males and females (Figures 2E and 2F).

Since mice in our aging study were older than the previously published paper on frailty (Whitehead et al., 2014), we tested whether individual frailty indicators show significant changes during this stage of aging. We applied the Mann-Kendall trend test to statistically assess if there is a monotonic upward or downward trend of frailty phenotype over time (Lento et al., 2012). Our results show that aging significantly increased the incidence of 11 and 14 frailty phenotypes in female and male, respectively (Figures 3A and 3B; Table S2). Among these phenotypes, the nasal discharge showed no changes upon aging. Also, grimace, distended abdomen, and breathing did not show any statistical trend in our analysis. We suggest that these three phenotypes are signs of imminent mortality and simply do not accumulate within the age bracket in this study. When an animal exhibits any of these

phenotypes, it will die within a few weeks. Therefore, although these phenotypes are age related, they do not show a trend with age.

Next, we tested the effects of CaAKG treatment on age-dependent phenotypes utilizing the mixed model (Figures 3C and 3D). CaAKG treatment significantly decreased the severity of multiple age-dependent phenotypes in females, including fur color loss, piloerection, poor coat condition, dermatitis, gait disorder, and kyphosis (Figure 3C). In males, severity of body condition, dermatitis, gait disorder, eye discharge, kyphosis, and tumors were all decreased (Figure 3D). Among the frailty measures affected by CaAKG, protection from age-related changes in female coat color was particularly prominent. We chose to characterize this phenotype in more detail by detecting dopachrome tautomerase (*Dct*), which is expressed in the differentiated melanocytes (MCs) of the hair bulb during anagen phase (Figure 3E).We found that 6 months of AKG supplementation can increase the population of MCs in skin sections (Figures 3F–3I). Gait improvement was also observed in both sexes. We further confirmed gait improvement utilizing metabolic cages. Physical activity and walking were simultaneously recorded over 4 consecutive days (Figures 3J and 3K). Interestingly, despite increased locomotion, the levels of oxygen consumption, carbon dioxide production, and energy expenditure were significantly lower in the CaAKG-treated group (Figure S4).

Not all phenotypes were improved by CaAKG. Treated mice failed to perform better in a treadmill exhaustion test and showed no cardiac functional improvement, as determined using echocardiography (Figure S4). Importantly, however, we did not detect any significant adverse changes with CaAKG treatment (Figure S2).

To gain better mechanistic insight, we initiated CaAKG treatment in a new cohort of female mice at 18 months of age. The reported beneficial effect of AKG on lifespan in *C. elegans* was associated with reduced TOR signaling (Chin et al., 2014). We did not detect any decrease in mTORC1 signaling upon three months of CaAKG treatment in different tissues of mice (Figure S5). However, these experiments were done in absence of any challenge to modify mTOR activity.

Age-associated diseases are accompanied by chronic inflammation, which is generally linked to an age-associated functional decline (Chung et al., 2009). We measured levels of 24 inflammatory cytokines in the serum of aged female mice (28 months old). In untreated mice, the levels of most cytokines increase; however, CaAKG-fed animals were largely refractory to these changes ($p < 0.0001$; Figure 4A). The reduction in inflammation is consistent with previous findings in the intestine of young pigs receiving an AKG supplementation (He et al., 2017). We repeated the same experiment in both sexes. Interestingly, 6 months of AKG treatment could only affect the cytokine levels in female mice (Figures 4B and S6).

In order to investigate the cytokine secretion profile of leukocytes, splenocytes were harvested and re-stimulated in culture. Splenic T cells from AKG-treated mice significantly produce higher interleukin (IL)-10; this effect was sex specific with higher levels in AKG-treated female mice (Figures 4C and 4D). IL-10 is a potent anti-inflammatory cytokine that

plays a central role in limiting host immune response (Ip et al., 2017). Considering the critical role of T cell mediated IL-10 in chronic inflammatory conditions (O'Garra et al., 2004), we believe that induction of IL-10 by AKG treatment can be a potential mechanism for suppression of chronic inflammation.

Studies have shown the accumulation of senescent cells in different tissues of old mice (van Deursen, 2014). These cells contribute to age-associated inflammation by acquiring the senescence-associated secretory phenotype (SASP), and their removal extends lifespan (Baker et al., 2011). We looked into senescent markers in different tissues of mice and did not detect any significant changes (Figures 4E and 4F). We further performed cell culture studies to explore possible effects of NaAKG in primary fibroblasts, a well-established model for cellular senescence (Campisi, 2013). While no changes in the senescence formation response to ionizing radiation were observed (Figure 4G), consistent with *in vivo* findings, AKG altered the SASP (Figures 4H and 4I). Specifically, we found a reduction of IL-1b, IL-6, CCL2, and MMP3 without any changes in β-gal and p21.

DISCUSSION

Maintaining function and health are primary outcomes of interest in longevity trials (Newman et al., 2016). A number of different frailty indices have been developed for humans. The most widely used scales are the "Fried frailty phenotype" (Fried et al., 2001) and the "Rockwood frailty index" (Rockwood et al., 2005). Howlett and colleagues have developed a simplified, noninvasive method to quantify frailty through health assessment of C57BL/6J mice. This index exhibits key features of the Rockwood frailty index, including similar exponential increases (Whitehead et al., 2014).

We repeatedly collected longitudinal health measurements and applied statistics to take into account the dependency of each dataset and the random nature of our study units (mice). Our findings demonstrate that AKG, a key metabolite in the TCA cycle, has longevity effects consistent with compressed morbidity in a long-term study of mouse aging. Notably, CaAKG administration started at 18 months of age had robust effects. This is valuable, as human clinical studies are likely to be initiated at a similar relative age. If translated to humans, this effect would be highly desirable, extending lifespan, but more importantly, reducing the debilitating period of functional decline and disease management.

Recent findings have shown that the SASP from senescent cells can drive age-related pathologies through paracrine and likely endocrine effects (Tanaka et al., 2018; Wiley et al., 2019). Our *in vitro* data indicate that AKG can alter the SASP and reduce inflammation without affecting the formation of senescent cells. Although this is consistent with our *in vivo* observation of reduced inflammation, there are additional sources of the observed cytokines such as tissue resident macrophages or other immune cells. Inhibition of SASP is a possible mechanism for AKG action in aging mice, and more confirmatory studies need to be performed. Also, senescent cells can activate inflammatory pathways in immune cells (Hall et al., 2016; Vicente et al., 2016), thus it is possible that immune cell activation, the SASP, or likely both are inhibited by AKG.

We show that female T cells significantly produce higher IL-10 upon AKG treatment. This effect, as well as suppression of inflammation and decreased mortality, were sex specific. Interestingly, IL-10 knockout (KO) mice (IL-$10^{tm/tm}$) show frailty phenotypes, such as an increase in several pro-inflammatory cytokines including IL-6, IL-1β, TNF-α, CXCL-1, and IL-12, as well as reduced muscle strength and higher mortality rates (Ko et al., 2012; Walston et al., 2008). IL-10 is produced by a variety of immune cell types; however, in context of chronic inflammation, the source of IL-10 is largely T cells (O'Garra et al., 2004). In addition, mice lacking IL-10 specifically in T cells recapitulate the immune phenotype of the whole-body IL-10 KO (Roers et al., 2004). Considering the critical role of T cell mediated IL-10 in chronic inflammatory conditions (O'Garra et al., 2004), we believe that induction of IL-10 by AKG treatment is a potential mechanism for suppression of chronic inflammation in females.

We observed no significant adverse effects of AKG administration. The only phenotypes that had a higher incidence in AKG-treated animals were cataracts and corneal opacity, although neither reached statistical significance. AKG has been used in human clinical studies linked to diseases without associated adverse effects (Filip et al., 2007; Jeevanandam and Petersen, 1999; Riedel et al., 1996). Interestingly, in humans, plasma AKG levels are reported to decline 10-fold between the ages of 40 and 80 (Harrison and Pierzynowski, 2008). The molecule is not available in the human diet, making direct supplementation the only feasible route to restore levels. Given its GRAS status and human safety record, our findings point to a potential safe human intervention that may impact important elements of aging and improve quality of life in the elderly population.

Limitations of Study

Our study has some limitations, and more research is needed to determine the causative mechanism underlying the longevity effects of AKG. While our data support increased IL-10 and reduced systemic inflammation as a potential longevity mechanism by AKG in females, this mechanism of action is absent in male animals. The applied frailty index lacks power to assess cognitive functions and behavior. Another limitation of the study is that the control diet lacked calcium. There is no data supporting the longevity effects of calcium treatment in mammals; however, this should be tested. It has been shown previously that the endogenous AKG levels in plasma decrease upon aging in mice and oral supplementation of AKG can restore levels (Tian et al., 2020); however, we did not quantify this in our study.

STAR★METHODS

RESOURCE AVAILABILITY

Lead Contact—Further information and requests for resources and reagents should be directed to and will be fulfilled by the Lead Contact, Brian K. Kennedy (bkennedy@nus.edu.sg).

Materials Availability—This study did not generate new unique reagents.

Data and Code Availability—The datasets and codes generated during this study are available at Mendeley [https://doi.org/10.17632/zr4ffhd3k9.1 and https://doi.org/10.17632/ytstmynn4m.1]. All other data are available from the corresponding author upon request.

EXPERIMENTAL MODEL AND SUBJECT DETAILS

Animals—Two independent cohorts of female and male C57BL6/J mice were purchased from Jackson Laboratories at 14 months of age (RRID: IMSR_JAX:000664). All mice were housed on a 12-h light/dark cycle and kept at 20–22°C. Animals were aged on a regular mouse diet (Teklad Irradiated 18% protein and 6% fat diet-2918) which is very similar to their diet at Jax 5K52 (18%–19% protein and 6%–7% fat) prior to arrival, until they reached 18th month of age when treatment started. AKG treated animals were subjected to a lifelong 2% (w/w) AKG supplement on 2918 diet while control group were kept on standard-2918 diet. Pure calcium 2-oxoglutarate was purchased from Carbosynth Company and homogeneously mixed during manufacturing of the 2918 diet prior to irradiation and pelleting. The exact sample size can be found in survival section. Mice were housed in groups (5 per cage at a maximum) and aggressive male mice were isolated to prevent fighting. All lifespan and healthspan experiments were started around 18th month of age. All the animals were scored before grouping and all the 31 scores were applied to assign animals into different groups. A balanced partitioning of mice was done: for any given mouse in any given group, there are similar mice in all other groups. This allows any outcome of the study to be more related to experiments or the treatment rather than the inherent property of a group.

Mice were inspected daily and treated for non-life-threatening conditions as directed by the veterinary staff. The only conditions that received treatment were dermatitis and prolapse (topical solution three times per week). Total of 8 mice in control group and 3 mice in AKG group were treated for dermatitis and prolapse. Each room contains sentinel mice (CD-1 females- 1 cage/75–100 cages). Health screening is done 4 times per year at 3 months intervals. Diagnostics consist of serological screening and fecal and fur analysis for internal and external parasites. All animal protocols were approved by Animal Care and Use Committee (A10217) of the Buck Institute. The Buck Institute is NIH/OLAW assured (D16–00624 (A4213–01)), and an AAALAC International accredited facility.

Cell Line—IMR-90 female fetal lung fibroblasts were obtained from ATCC (RRID: CVCL0347) and were cultured at 37°C in 3% O2and 5% CO2. Dulbecco’s modified Eagle’s media (DMEM) supplemented with 10% fetal bovine serum and streptomycin/penicillin were used. Media was changed every 2 days during the experiment. The authentication was done by ATCC.

METHOD DETAILS

Survival—The principle endpoint of lifespan study was natural death. We recorded the age at which mice were found dead or selected for euthanasia (a procedure for mice deemed unlikely to survive for the next 48 h and are in enormous discomfort). The criteria for euthanasia was based on an independent assessment by a veterinarian, according to AAALAC guidelines and only where the condition of the animal was considered (Harrison

et al., 2009). Severe lethargy, rapid weight loss (over two weeks > 20%), severe distended abdomen and body condition score with signs of pain (grimace), inability to move despite the stimuli, severe ulcer or bleeding tumor, severe temperature loss with abnormal breathing rate. Animals found dead or euthanized were necropsied for pathology score. Mice either received Teklad-2918 or 2% w/w AKG supplemented 2918. Cohort-1 consists of female control (n = 24), female AKG (n = 20), male control (n = 24) and male AKG (n = 22) animals. Cohort-2 consists of female control (n = 23), female AKG (n = 23), male control (n = 24) and male AKG (n = 23) animals. No invasive measurements were performed on this population, n = 183 animals (two cohorts of 90 animals). Two sacrificed group were purchased at 14th months of age, baselined and grouped the following week. The first group was sacrificed after 3 months of AKG supplementation and consisted of 12 female mice (6 mice per treatment). The second group was sacrificed after 6 months of supplementation and consisted of 20 mice which included both sexes (5 mice per treatment per sex). The Institutional Animal Care and Use Committee (IACUC) at the Buck Institute approved all animal experimental procedures, housing and diets for Research on Aging. Food intake and body weight were measured on a biweekly and bimonthly basis for the duration of the study.

Baselining and Grouping of the Animals—Mammals age heterogeneously and the 18 months old mice already manifest some age-associated deterioration of health phenotypes. All the animals were scored before grouping and all the 31 scores were applied to assign animals into different groups. A balanced partitioning of mice was done: for any given mouse in any given group, there are similar mice in all other groups. This allows any outcome of the study to be more related to experiments or the treatment rather than the inherent property of a group.

Aging Index (Frailty Index)—One can find the complete protocol as published before by Whitehead et al., 2014. For the subjective properties of the assessments, all measurements were completely blinded.

These assessments indicate age-associated deterioration of health and include evaluation of the animal musculoskeletal system, the vestibulocochlear/auditory systems, the ocular and nasal systems, the digestive system, the urogenital system, the respiratory system, signs of discomfort, body weight and body surface temperature. 0 is assigned if no sign of frailty is observed and the animal is healthy for that phenotype. A moderate phenotype and a severe phenotype will be scored 0.5 and 1 respectively. Loss of temperature and weight were scored using standard deviation for our study (Figure S1). We should note that the recessive *Cdh23* allele (*ahl*) in C57BL/6J strain, when homozygous, leads to increased susceptibility to age-related hearing loss. Hearing loss was one of the most abundant aging phenotypes in our dataset.

Skin Collection and Melanocyte Synchronization—Mice were waxed in the dorsal area (area of 1.5 inches × 2 inches) to initiate the hair cycle and start a homogeneous re-entry into anagen. Seven days later skin samples were collected and were immersed in 4% paraformaldehyde/PBS (pH 7.4) and immersed in 30% sucrose for few days until the samples sank to the end of the tubes. The fixed skin was embedded in OCT compound and snap-frozen (Nishimura et al., 2002). For double or triple immunofluorescent staining, 14

microm cryosections were acquired. After treatment with a blocking solution containing 5% skim milk (Difco), 1% donkey serum and 0.1% Triton X-100 for 20 in PBS, skin sections were incubated with primary Rabbit polyclonal to TRP2 (Dct) Antibody (abcam) diluted in the blocking solution. The sections were then washed three times in PBS containing 0.1% Triton X-100. Skin sections were incubated with Alexa488-conjugated donkey anti-rabbit IgG diluted in blocking solution containing DAPI. After washing three times with PBS, the slides were mounted with a ProLong Antifade kit (Molecular Probes) and observed under a confocal microscope (Bio-Rad Radiuns 2100 or Zeiss LSM510 Meta).

Metabolic Data (Physical Activity)—Metabolism was measured applying indirect Calorimetry. We used Promethion metabolic cage system-Sable Systems International. The system is equipped with GA-3 small mammal gas analyzers for measurements of O2 (consumption) and CO2 (production). Energy expenditure, food intake, water consumption, body weight, physical activity and volunteer exercise were simultaneously recorded over 4 consecutive days (96 h). Mice were housed individually in metabolic cages and accustomed to their environment a day before the start of recording. Data were analyzed using Sable System Expedata-P Data Analysis Software. Subsequently, we applied CalR software, a free web tool for analysis of experiments using indirect calorimetry (Mina et al., 2018), to analyze our raw data, generate some of our plots and run statistical analysis (https://calrapp.org). The whole-body composition analysis was conducted using a quantitative nuclear magnetic resonance machine (EchoMRI-2012, Echo Medical Systems).

Inflammatory Cytokines and Chemokines—Blood were from the jugular vein of young (18 months old), aged control and AKG fed (29 months old) animals. The samples were sent to Eve technologies (Calgary, Alberta, Canada) for measurement of soluble cytokines and chemokines in serum using multiplex lase bead array technology (MD31)

Spleen Cytokine Expression (Flow Cytometry Procedure)—After 6 months of AKG treatment, animals were sacrificed. Leukocyte suspensions were prepared from mouse spleens by crushing, dissociation of cells by pipetting, straining through 40-micron nylon mesh, and ACK lysis. For analysis of cytokine expression, cells were cultured in RPMI/10% FCS for 4 h post-isolation, with 50ng/mL PMA (Sigma), 0.5 μM ionomycin (Sigma), and 0.5 μg/mL Brefeldin A (Sigma) prior to staining. Surface staining with fluorochrome-conjugated antibodies was performed for 30 min on ice, at 1 μg/mL, in PBS with 2% FCS and 2mM EDTA, followed by either fixation in PBS/1% PFA or fixation/permeabilization with the eBioscience (ThermoFisher) FOXP3 intracellular staining kit. Intracellular staining for cytokines or transcription factors was performed for 1 h on ice in eBioscience FOXP3 Perm/wash buffer. Samples were analyzed using a BD LSR II flow cytometer. All antibodies for flow cytometry were obtained from Biolegend and are all listed in Key Resources Table.

Cell Culture—For damage-induced senescence, cells were irradiated with doses of either 0 or 10 Gy of ionizing radiation (IR). Cells were concurrently treated with PBS (control) or 1 mM AKG for 10 days, changing media every 2 days. All assays were performed 10 days post irradiation.

EdU (5-ethynyl-2′-deoxyuridine) staining Proliferation Kit (iFluor 488) ab219801 was used to detect cell proliferation. Cells were stained for the senescence-associated β-gal (SA-β-gal) marker as described (Dimri et al., 1995). Non-senescent cells (having under-gone fewer than 35 population doublings) were made quiescent by washing with PBS and incubating in DMEM containing 0.2% serum for 4 day. Cultures that had > 80% SA-β-gal positive cells and ≤ 4% EdU positive cells were considered senescent.

ELISA—Conditioned media were prepared by washing cells 3 times in PBS and incubating them in serum-free DMEM containing penicillin/streptomycin for 24 h. Conditioned media were removed and cells were trypsinized for cell counts. The conditioned media were then centrifuged to remove cellular debris, and supernatants were used for ELISA. IL-6 ELISA were performed using R&D systems Human IL-6 Detection Kit and procedures (#HS600C). The result data were normalized to cell number.

RT PCR—For cell culture experiments, RNA was isolated using ISOLATE II RNA mini kit (Bioline #BIO-52073). RNA quality and quantity were assessed using NanoDropTM 1000 Spectrophotometer measures (Thermo Scientific). Total cDNAs were synthesized from 500ng of RNA using random primers and iScript RT reagents following the manufacturer's protocol Superscript II (Invitrogen, Carlsbad, USA). Gene expression was measured from cDNA using the Roche Universal Probe Library system (Indianapolis, IN, USA). All values were normalized to beta-actin.

For *in vivo* study tissues were collected form 12 animals described as sacrificed group. Tissues were homogenized in 1 mL Invitrogen TRIzol Reagent using metal beads combined with high-speed shaking (Tissuelyser QIAGEN at 20 Hrtz, for 6 min). Skin samples were crushed with pistol and liquid nitrogen prior to homogenizing step. The chloroform extraction and ethanol precipitation were performed on homogenized tissues to extract RNA. The RNA quality and quantity were assessed and cDNA were synthesized as described. Gene expression was quantified by real-time quantitative PCR using the Roche Universal Probe Library system (Indianapolis, IN, USA). The primer sets are presented in Key Resources Table (Table S3).

Transthoracic Echocardiography—Transthoracic echocardiography Echocardiography examination was performed using a high resolution (32–55 MHz) Visualsonics Vevo 2100 micro-ultrasound system with the echocardiography probe (MS-400). Individual mouse was placed on a heating pad (37°C) and minor sedation (0.5% isoflurane oxygen) was used to paralyze the animal (minimizing the cardiac suppression side effect) during the measurement time. Doppler imaging, 2D and M-mode echocardiography was performed to evaluate cardiac morphometry, systolic function, and Mean baseline myocardial performance index (MPI).

Treadmill Exhaustion Test—We modified the protocol by Castro et al., 2017(Castro and Kuang, 2017). Since, mice were old (28th month-old) the initial speed and the acceleration were adjusted for our study. All mice were trained and adapted to the environment for three consecutive days for 10 min at 5 m/min before the actual experiment. On the day of experiment mice were warmed up for 3 min at 5 m/min after which the speed was

accelerated by 1.5 m/min^{-2}. We used air puff as stimuli to keep the animal running. The maximal speed and distance were recorded once the mice were exhausted (signs of exhaustion including heavy breathing, hunched back and unwillingness of the animal to get on the treadmill belt despite of 10 air puffs).

Western—Mouse were fasted overnight, the next morning tissues; heart, lung, kidney, adipose tissue (visceral fat in females, carefully along the epididymis and the uterus) and skin (back skin, on the spine midway between the head and the tail) were dissected and immediately frozen in liquid nitrogen. Tissues were homogenized using the Omni TH homogenizer (Omni International) on ice in Radioimmuno-precipitation assay (RIPA) buffer; 300 mM NaCl, 1.0% NP-40, 0.5% sodium deoxycholate, 0.1% SDS, 50 mM Tris (pH 8.0), protease inhibitor cocktail (Roche) and phosphatase inhibitor 2, 3 (Sigma). Samples were centrifuged at 13,200 rpm for 10 min, 4°C. The protein contents of the supernatants were assessed using the detergent compatible (DC) protein assay (Bio-Rad). Equal amounts of protein were resolved by SDS-PAGE (4%– 12% Bis-Tris gradient gel, Invitrogen), transferred to nitrocellulose membranes, and incubated with protein/phosphoprotein-specific antibodies. The antibodies against phosphorylated-S6 (S240/244), Akt (Ser473), S6, Akt, and glyceraldehyde 3-phosphate dehydrogenase (GAPDH) were purchased from Cell Signaling Technology (Key Resources Table). Protein bands were revealed using the Amersham enhanced chemiluminescence (ECL) detection system (GE Healthcare) and quantified by ImageJ software.

QUANTIFICATION AND STATISTICAL ANALYSIS

Python Software was used to extract all the recorded healthspan data and create files compatible with software for analysis. Data were analyzed using R version 3.3.3, GraphPad Prism 8 and OASIS 2 software (Han et al., 2016). Log-rank (Mantel–Cox) tests were used to analyze Kaplan–Meier curves, and a Fisher's exact test was performed for maximum lifespan analysis (at 90% survival). We applied Mixed models analysis for our longitudinal frailty data in both Prism 8 and R. In the current Mixed Model, every mouse with a unique ID were treated as a random effects, treatment and time were treated as fixed effect: R packages "lme4" and "lmerTest" were used, R codes are uploaded in resources table. The repeated-measure correlation was applied to analyze correlation in our longitudinal dataset. The mixed model was utilized for comparison of the slope of the regression lines. The R packages "rmcorr,""lme4" and "gplot2" for graphing were used. The Mann-Kendall Trend Test was applied to check for possible monotonic changes in frailty over time (age-dependent frailty phenotypes): The R package "Kendall" and "trend" were used. All R codes are available in resources table. Two-way analysis of variance (ANOVA) was used for analysis between morbidity curves. The area under curve (AUC) of mortality graphs were measured baselining at 18 months of age. The changes in AUC were used to calculate the percent compression of morbidity. Non-parametric Two-tailed Student's t tests were used for analyses of scoring at each time point between control and AKG treated group. All of the statistical details of experiments including sample size, sex, age and the applied statistical method can be found in the figure legends and Results section. Significance was defined for P values smaller than 0.05: *$p < 0.05$, **$p < 0.01$, ***$p < 0.001$ and ****$p < 0.0001$.

Supplementary Material

Refer to Web version on PubMed Central for supplementary material.

ACKNOWLEDGMENTS

This work was supported by The Weldon Foundation and by Ponce de Leon Health. This work was also supported by NIH grant U01AG045844 (G.J.L.), NIA grant R01AG051729, grant support from the Larry L. Hillblom Foundation, and the Navigage Foundation. We thank Susan Howlett for initial guidance and help to establish the frailty index measurements at Buck. We also thank John Newman, Douglas R. Seals, and all the members of the Lithgow and Kennedy labs for their input on writing the paper.

REFERENCES

Bakdash JZ, and Marusich LR (2017). Repeated Measures Correlation. Front. Psychol 8, 456. [PubMed: 28439244]

Baker DJ, Wijshake T, Tchkonia T, LeBrasseur NK, Childs BG, van de Sluis B, Kirkland JL, and van Deursen JM (2011). Clearance of p16Ink4a-positive senescent cells delays ageing-associated disorders. Nature 479, 232–236. [PubMed: 22048312]

Bansal A, Zhu LJ, Yen K, and Tissenbaum HA (2015). Uncoupling lifespan and healthspan in Caenorhabditis elegans longevity mutants. Proc. Natl. Acad. Sci. USA 112, E277–E286. [PubMed: 25561524]

Bland JM, and Altman DG (1995). Calculating correlation coefficients with repeated observations: Part 1–Correlation within subjects. BMJ 310, 446. [PubMed: 7873953]

Campisi J (2013). Aging, cellular senescence, and cancer. Annu. Rev. Physiol 75, 685–705. [PubMed: 23140366]

Castro B, and Kuang S (2017). Evaluation of Muscle Performance in Mice by Treadmill Exhaustion Test and Whole-limb Grip Strength Assay. Bio. Protoc 7, 10.21769/BioProtoc.2237.

Chin RM, Fu X, Pai MY, Vergnes L, Hwang H, Deng G, Diep S, Lomenick B, Meli VS, Monsalve GC, et al. (2014). The metabolite α-ketoglutarate extends lifespan by inhibiting ATP synthase and TOR. Nature 510, 397–401. [PubMed: 24828042]

Chung HY, Cesari M, Anton S, Marzetti E, Giovannini S, Seo AY, Carter C, Yu BP, and Leeuwenburgh C (2009). Molecular inflammation: underpinnings of aging and age-related diseases. Ageing Res. Rev 8, 18–30. [PubMed: 18692159]

Dimri GP, Lee X, Basile G, Acosta M, Scott G, Roskelley C, Medrano EE, Linskens M, Rubelj I, Pereira-Smith O, et al. (1995). A biomarker that identifies senescent human cells in culture and in aging skin in vivo. Proc. Natl. Acad. Sci. USA 92, 9363–9367. [PubMed: 7568133]

Filip RS, Pierzynowski SG, Lindegard B, Wernerman J, Haratym-Maj A, and Podgurniak M (2007). Alpha-ketoglutarate decreases serum levels of C-terminal cross-linking telopeptide of type I collagen (CTX) in postmenopausal women with osteopenia: six-month study. Int. j. vitam. nutr. res 77, 89–97. [PubMed: 17896582]

Fried LP, Tangen CM, Walston J, Newman AB, Hirsch C, Gottdiener J, Seeman T, Tracy R, Kop WJ, Burke G, and McBurnie MA (2001). Frailty in older adults: evidence for a phenotype. J. Gerontol. A Biol. Sci. Med. Sci 56, M146–M156. [PubMed: 11253156]

Friedman DB, and Johnson TE (1988). A mutation in the age-1 gene in Caenorhabditis elegans lengthens life and reduces hermaphrodite fertility. Genetics 118, 75–86. [PubMed: 8608934]

Hahm JH, Kim S, DiLoreto R, Shi C, Lee SJ, Murphy CT, and Nam HG (2015). C. elegans maximum velocity correlates with healthspan and is maintained in worms with an insulin receptor mutation. Nat. Commun 6, 8919. [PubMed: 26586186]

Hall BM, Balan V, Gleiberman AS, Strom E, Krasnov P, Virtuoso LP, Rydkina E, Vujcic S, Balan K, Gitlin I, et al. (2016). Aging of mice is associated with p16(Ink4a)- and β-galactosidase-positive macrophage accumulation that can be induced in young mice by senescent cells. Aging (Albany N.Y.) 8, 1294–1315.

Han SK, Lee D, Lee H, Kim D, Son HG, Yang JS, Lee SV, and Kim S (2016). OASIS 2: online application for survival analysis 2 with features for the analysis of maximal lifespan and healthspan in aging research. Oncotarget 7, 56147–56152. [PubMed: 27528229]

Hansen M, and Kennedy BK (2016). Does Longer Lifespan Mean Longer Healthspan? Trends Cell Biol. 26, 565–568. [PubMed: 27238421]

Harrison AP, and Pierzynowski SG (2008). Biological effects of 2-oxoglutarate with particular emphasis on the regulation of protein, mineral and lipid absorption/metabolism, muscle performance, kidney function, bone formation and cancerogenesis, all viewed from a healthy ageing perspective state of the art–review article. J. Physiol. Pharmacol 59 (Suppl 1), 91–106.

Harrison DE, Strong R, Sharp ZD, Nelson JF, Astle CM, Flurkey K, Nadon NL, Wilkinson JE, Frenkel K, Carter CS, et al. (2009). Rapamycin fed late in life extends lifespan in genetically heterogeneous mice. Nature 460, 392–395. [PubMed: 19587680]

He L, Zhou X, Huang N, Li H, Cui Z, Tian J, Jiang Q, Liu S, Wu J, Li T, et al. (2017). Administration of alpha-ketoglutarate improves epithelial restitution under stress injury in early-weaning piglets. Oncotarget 8, 91965–91978. [PubMed: 29190890]

Ip WKE, Hoshi N, Shouval DS, Snapper S, and Medzhitov R (2017). Anti-inflammatory effect of IL-10 mediated by metabolic reprogramming of macrophages. Science 356, 513–519. [PubMed: 28473584]

Jeevanandam M, and Petersen SR (1999). Substrate fuel kinetics in enterally fed trauma patients supplemented with ornithine alpha ketoglutarate. Clin. Nutr 18, 209–217. [PubMed: 10578020]

Kane AE, Hilmer SN, Boyer D, Gavin K, Nines D, Howlett SE, de Cabo R, and Mitchell SJ (2016). Impact of Longevity Interventions on a Validated Mouse Clinical Frailty Index. J. Gerontol. A Biol. Sci. Med. Sci 71, 333–339. [PubMed: 25711530]

Kenyon C, Chang J, Gensch E, Rudner A, and Tabtiang R (1993). A C. elegans mutant that lives twice as long as wild type. Nature 366, 461–464. [PubMed: 8247153]

Ko F, Yu Q, Xue QL, Yao W, Brayton C, Yang H, Fedarko N, and Walston J (2012). Inflammation and mortality in a frail mouse model. Age (Dordr.) 34, 705–715. [PubMed: 21633802]

Lento J, Dillon PJ, and Somers KM (2012). Evaluating long-term trends in littoral benthic macroinvertebrate communities of lakes recovering from acid deposition. Environ. Monit. Assess 184, 7175–7187. [PubMed: 22193633]

Mina AI, LeClair RA, LeClair KB, Cohen DE, Lantier L, and Banks AS (2018). CalR: A Web-Based Analysis Tool for Indirect Calorimetry Experiments. Cell Metab 28, 656–666.e1. [PubMed: 30017358]

Myllyharju J (2003). Prolyl 4-hydroxylases, the key enzymes of collagen biosynthesis. Matrix Biol. 22, 15–24. [PubMed: 12714038]

Newman JC, Milman S, Hashmi SK, Austad SN, Kirkland JL, Halter JB, and Barzilai N (2016). Strategies and Challenges in Clinical Trials Targeting Human Aging. J. Gerontol. A Biol. Sci. Med. Sci 71, 1424–1434. [PubMed: 27535968]

Nishimura EK, Jordan SA, Oshima H, Yoshida H, Osawa M, Moriyama M, Jackson IJ, Barrandon Y, Miyachi Y, and Nishikawa S (2002). Dominant role of the niche in melanocyte stem-cell fate determination. Nature 416, 854–860. [PubMed: 11976685]

O'Garra A, Vieira PL, Vieira P, and Goldfeld AE (2004). IL-10-producing and naturally occurring CD4+ Tregs: limiting collateral damage. J. Clin. Invest 114, 1372–1378. [PubMed: 15545984]

Parks RJ, Fares E, Macdonald JK, Ernst MC, Sinal CJ, Rockwood K, and Howlett SE (2012). A procedure for creating a frailty index based on deficit accumulation in aging mice. J. Gerontol. A Biol. Sci. Med. Sci 67, 217–227. [PubMed: 22021390]

Riedel E, Nündel M, and Hampl H (1996). alpha-Ketoglutarate application in hemodialysis patients improves amino acid metabolism. Nephron 74, 261–265. [PubMed: 8893139]

Rockwood K, Song X, MacKnight C, Bergman H, Hogan DB, McDowell I, and Mitnitski A (2005). A global clinical measure of fitness and frailty in elderly people. CMAJ 173, 489–495. [PubMed: 16129869]

Rockwood K, Blodgett JM, Theou O, Sun MH, Feridooni HA, Mitnitski A, Rose RA, Godin J, Gregson E, and Howlett SE (2017). A Frailty Index Based On Deficit Accumulation Quantifies Mortality Risk in Humans and in Mice. Sci. Rep 7, 43068. [PubMed: 28220898]

Roers A, Siewe L, Strittmatter E, Deckert M, Schlüter D, Stenzel W, Gruber AD, Krieg T, Rajewsky K, and Müller W (2004). T cell-specific inactivation of the interleukin 10 gene in mice results in enhanced T cell responses but normal innate responses to lipopolysaccharide or skin irritation. J. Exp. Med 200, 1289–1297. [PubMed: 15534372]

Schneider CA, Rasband WS, and Eliceiri KW (2012). NIH Image to ImageJ: 25 years of image analysis. Nature Methods 9, 671–675. [PubMed: 22930834]

Su Y, Wang T, Wu N, Li D, Fan X, Xu Z, Mishra SK, and Yang M (2019). Alpha-ketoglutarate extends *Drosophila* lifespan by inhibiting mTOR and activating AMPK. Aging (Albany N.Y.) 11, 4183–4197.

Tanaka T, Biancotto A, Moaddel R, Moore AZ, Gonzalez-Freire M, Aon MA, Candia J, Zhang P, Cheung F, Fantoni G, et al. ; CHI consortium (2018). Plasma proteomic signature of age in healthy humans. Aging Cell 17, e12799. [PubMed: 29992704]

TeSlaa T, Chaikovsky AC, Lipchina I, Escobar SL, Hochedlinger K, Huang J, Graeber TG, Braas D, and Teitell MA (2016). α-Ketoglutarate Accelerates the Initial Differentiation of Primed Human Pluripotent Stem Cells. Cell Metab. 24, 485–493. [PubMed: 27476976]

Tian Q, Zhao J, Yang Q, Wang B, Deavila JM, Zhu MJ, and Du M (2020). Dietary alpha-ketoglutarate promotes beige adipogenesis and prevents obesity in middle-aged mice. Aging Cell 19, e13059. [PubMed: 31691468]

Tsukada Y, Fang J, Erdjument-Bromage H, Warren ME, Borchers CH, Tempst P, and Zhang Y (2006). Histone demethylation by a family of JmjC domain-containing proteins. Nature 439, 811–816. [PubMed: 16362057]

van Deursen JM (2014). The role of senescent cells in ageing. Nature 509, 439–446. [PubMed: 24848057]

Vicente R, Mausset-Bonnefont AL, Jorgensen C, Louis-Plence P, and Brondello JM (2016). Cellular senescence impact on immune cell fate and function. Aging Cell 15, 400–406. [PubMed: 26910559]

Walston J, Fedarko N, Yang H, Leng S, Beamer B, Espinoza S, Lipton A, Zheng H, and Becker K (2008). The physical and biological characterization of a frail mouse model. J. Gerontol. A Biol. Sci. Med. Sci 63, 391–398. [PubMed: 18426963]

Whitehead JC, Hildebrand BA, Sun M, Rockwood MR, Rose RA, Rockwood K, and Howlett SE (2014). A clinical frailty index in aging mice: comparisons with frailty index data in humans. J. Gerontol. A Biol. Sci. Med. Sci 69, 621–632. [PubMed: 24051346]

Wiley CD, Liu S, Limbad C, Zawadzka AM, Beck J, Demaria M, Artwood R, Alimirah F, Lopez-Dominguez JA, Kuehnemann C, et al. (2019). SILAC Analysis Reveals Increased Secretion of Hemostasis-Related Factors by Senescent Cells. Cell Rep. 28, 3329–3337.e5. [PubMed: 31553904]

Wood JG, Rogina B, Lavu S, Howitz K, Helfand SL, Tatar M, and Sinclair D (2004). Sirtuin activators mimic caloric restriction and delay ageing in metazoans. Nature 430, 686–689. [PubMed: 15254550]

Wu L (2010). Mixed Effects Models for Complex Data (Chapman & Hall/CRC Press).

Zdzisińska B, Żurek A, and Kandefer-Szerszeń M (2017). Alpha-Ketoglutarate as a Molecule with Pleiotropic Activity: Well-Known and Novel Possibilities of Therapeutic Use. Arch. Immunol. Ther. Exp. (Warsz.) 65, 21–36. [PubMed: 27326424]

Highlights

- A CaAKG-supplemented diet extends lifespan of middle-aged female mice
- AKG supplementation extends healthspan of both female and male mice
- AKG compresses morbidity. Reduction in frailty is more dramatic than lifespan extension
- AKG reduces chronic inflammation and induces IL-10 in T cells of female mice

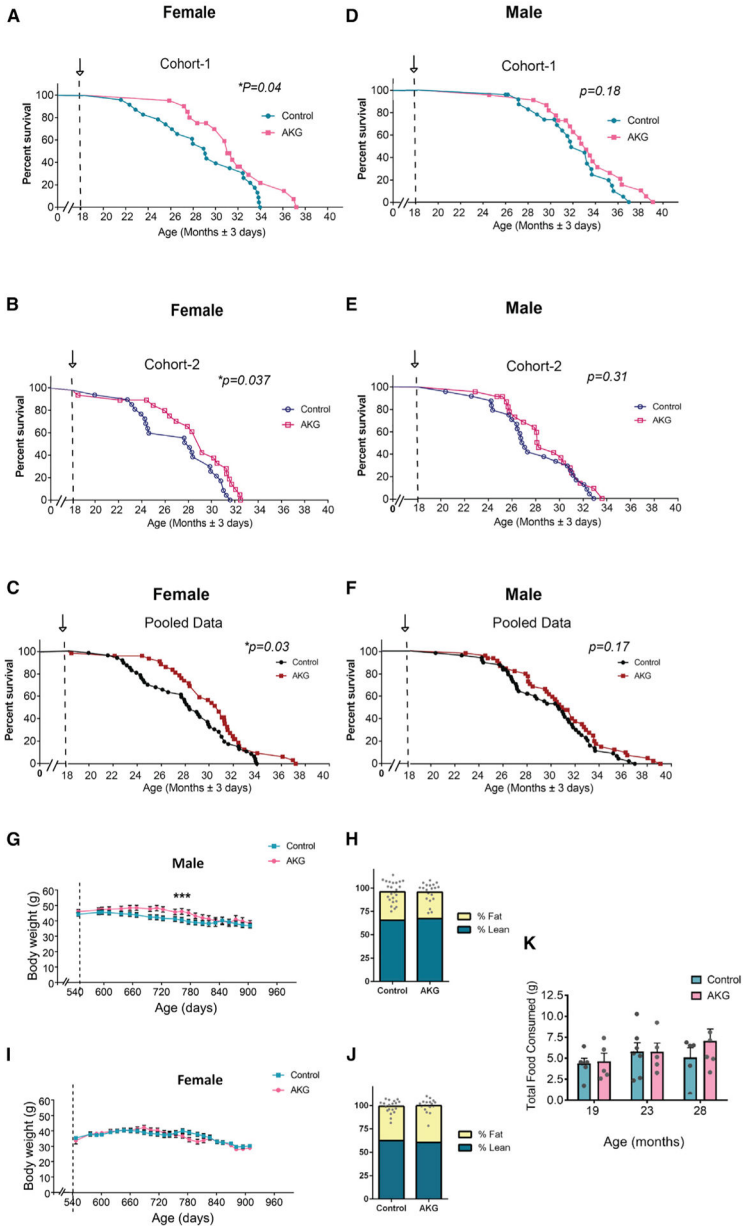

Figure 1. AKG Extends Lifespan and Decreases Mortality

Post-treatment survival plots graphed for cohort 1 (n = 90) and cohort 2 (n = 93). Comparing control mice to those fed AKG in the diet starting at 18 months of age. Arrows indicate the start of the treatment.

(A–C) Female survival curves for cohort 1 (A) control (n = 24), AKG (n = 20) and cohort 2 (B) control (n = 23), AKG (n = 23), and (C) pooled females.

(D–F) Male survival curves for cohort 1 (D) control (n = 24), AKG (n = 22) and cohort 2 (E) control (n = 24), AKG (n = 23), and (F) pooled males. Survival curve comparisons were performed using Log-rank test; *p < 0.05. Maximum lifespan extensions were calculated using Fisher's exact test statistics; **p = 0.0064 for female cohort 1 and *p < 0.021 for female cohort 2.

(G and I) Body weight trajectories from cohort 2 mice; n = all live animals in the study at each time point; data are mean ± SEM. Two-way ANOVA tests were applied to check if independent variables including time and treatment (AKG) affect male and female body weight. The comparison provided evidence of significant effects of both treatment and time on male body weight; ***$p < 0.0001$, ***$p < 0.001$, and effect of only time on female body weight ***$p < 0.001$.

(H and J) Male (H) and female (J) body composition; n = all live animals in the study; data are mean ± SEM; no significance changes detected (two-tailed t test).

(K) Food consumption was measured for 3 consecutive days in different times during the lifespan of female control (n = 6) and female AKG-fed (n = 5) mice; the arrows at 19, 23, and 28 months show the age at which food consumption was measured. Data are mean ± SEM; no significance change (two-tailed t test).

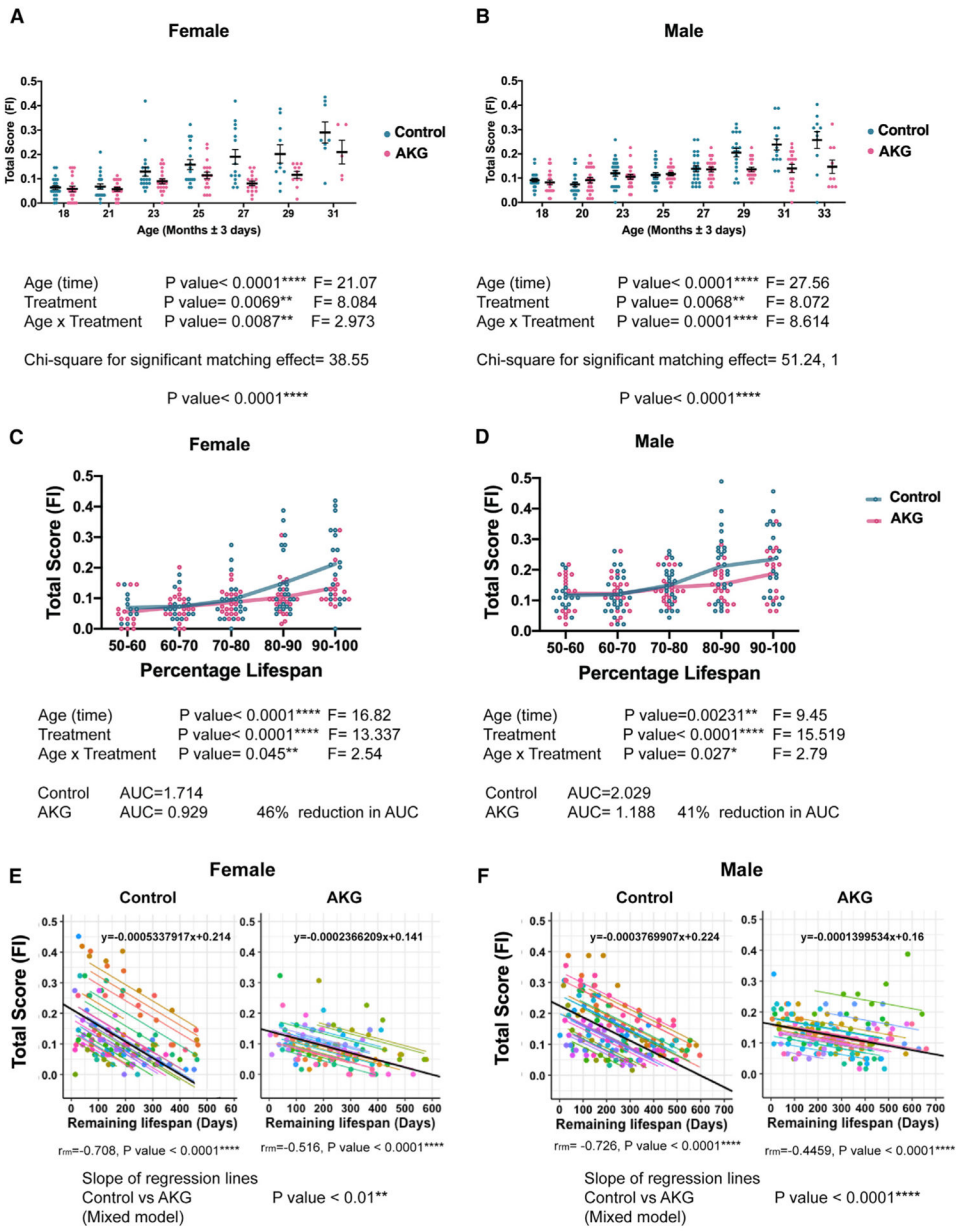

Figure 2. Compression of Morbidity by AKG Treatment

(A and B) Separately graphed (A) female and (B) male total frailty index (FI) scores during lifespan, comparing control mice (blue) to those fed AKG in the diet (pink) starting at the 18th month. Each dot is the total score of one animal at specific age as indicated. Data are mean ± SEM of each group. n = all animals alive at each measurement time. Mixed model was used to analyze the data longitudinally. In the current mixed model, every mouse with a unique ID was treated as a random effect. Treatment and time were treated as fixed effects. The low p value for chi-square for significant matching effect indicates that the pairing was effective; comparing the fit of the current mixed model to a simpler ANOVA, ****$p < 0.0001$. As the animal ages and gets closer to death (higher percentage of lifespan),

it manifests several aging phenotypes and will be at its highest multi-morbidity risk. We considered the total scores of 31 phenotypes as a morbidity score.
(C and D) Separately graphed (C) female and (D) male mice total FI scores as their percentage of lifespan. AKG treatment postpones the occurrence of aging phenotypes during lifespan and compresses the morbidity risk into fewer days of life in both sexes. Each dot is the total score of one animal. Lines are mean ± SEM of the group. n = all animals alive at each time. Two-way ANOVA was used for comparison. The area under the frailty curves (AUC) were calculated to measure the percent comparison of morbidity.
(E and F) The total scores for each mouse were plotted against remaining life (life expectancy). Repeated-measures correlation (rmcorr) was applied for AKG and control groups separately and rmcorr coefficients (r_{rm}), and associated p values have been indicated. Dots and specific regression lines for each mouse with unique ID are color coded. There are negative correlations between total score and life expectancy in both control and AKG for both sexes. We also reported the slopes of the regression lines, which computed by rmcorr for AKG and control separately (black lines). The equation of each regression line is shown ($y = ax + b$). Where x is the explanatory variable, a is the slope of the line, and b is the intercept. The results suggest a decrease in magnitude of slope for AKG treatment compared to control. To further prove that this difference is statically meaningful, we applied a mixed model to the combined dataset of AKG and control. In the current mixed model, we treated remaining life and treatment as fixed effects and every mouse as a random effect. The reported p value for regression lines is the result of analysis of variance (ANOVA) for the slopes. AKG treatment can significantly decrease the rate of linear relationship between life expectancy and total score in both males and females.

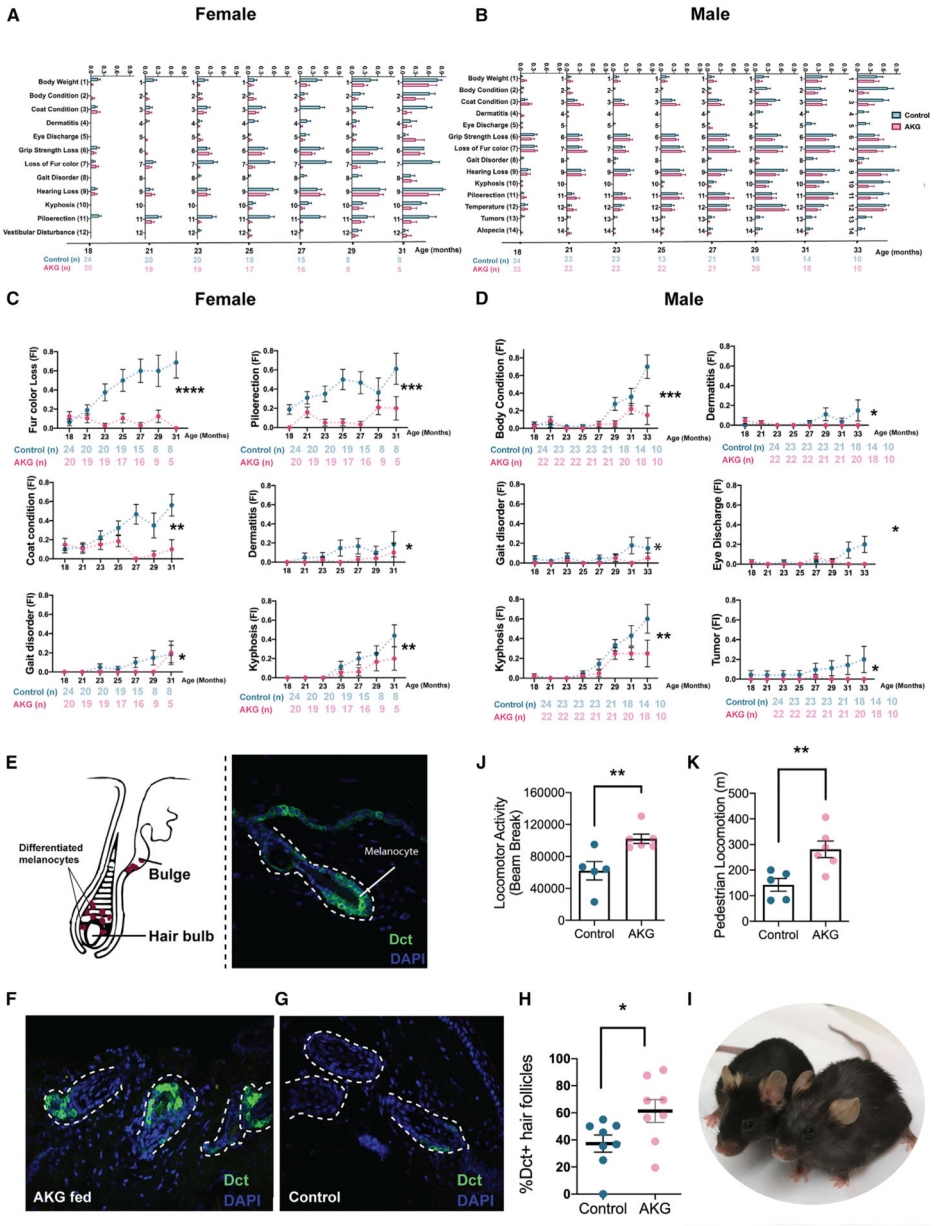

Figure 3. AKG Treatment Extends Healthspan and Alleviates Age-Associated Frailty

(A and B) Individually graphed frailty phenotypes that significantly increase with aging, comparing control with AKG treated mice for (A) female and (B) male. The number of animals assessed at each time point are shown as row beneath each graph. Data are mean ± SEM of the group.

(C and D) Trajectories for age-dependent frailty phenotypes for (C) female and (D) male in the study. Mixed model was used to test if each age-dependent phenotype was affected by AKG supplementation. *p < 0.05, **p < 0.01, ***p < 0.001, ****p < 0.0001. See also Figure S3.

(E) Simplified anatomy of an anagen hair follicle showing the location of differentiated melanocytes in hair bulb with corresponding immunofluorescence image.

(F and G) Phenotypical characterization of melanocytes in the hair matrix during anagen phase for (F) female AKG-treated and (G) female control mice after 6 months of treatment. Skin sections were stained with antibodies against Dct. nuclear staining (blue) with DAPI.
(H) Dot plot showing the percentage of Dct+ hair follicles in skin sections. Data are mean ± SEM of the group. *$p < 0.05$ (two-tailed t test).
(I) Aged-matched control (right) and AKG-fed (left) female mice. Animals are 28 months old in the captured picture.
(J and K) Locomotor activity (J) and pedestrian locomotion (K) were measured utilizing metabolic cages at the median life (28 months old) of female control (n = 5) and female AKG (n = 6) mice. Total locomotor activity refers to any movement made by the animal that is picked up by the sensors. The pedestrian locomotion is referred to walking. Data are mean ± SEM; **$p < 0.001$ (two-tailed t test).

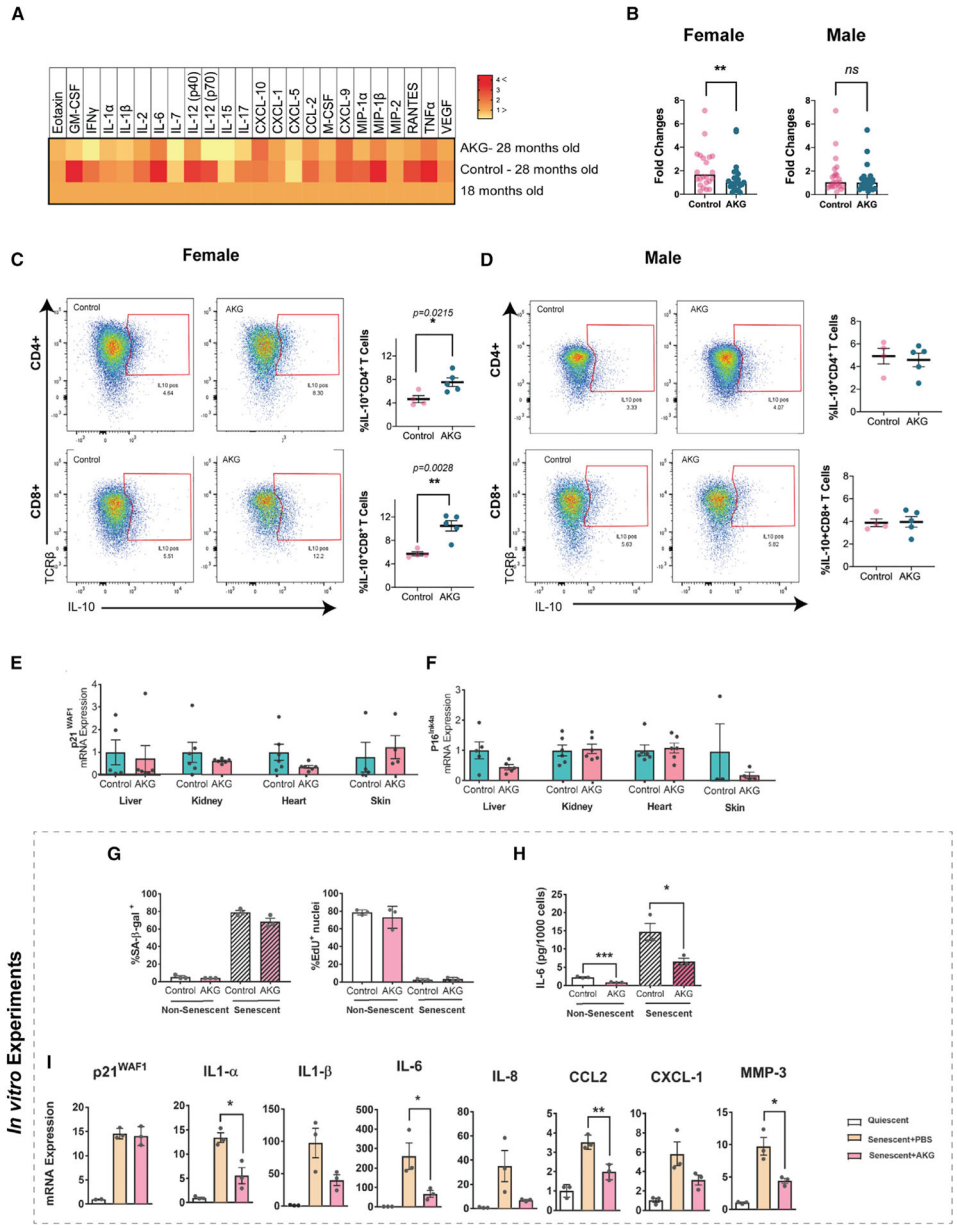

Figure 4. AKG Reduces Inflammation

(A) Heatmap of 24 inflammatory cytokines and chemokines from the plasma of middle-aged (female, age = 18 months, n = 11), aged control, and AKG (female, 28 months old, n = 5) animals. Inflammatory cytokines show a general trend of reductions in AKG group compared to aged control.

(B) Fold changes of 24 inflammatory cytokines for female and male mice after 6 months of treatment (24 months old, n = 5). Levels were calculated using the untreated 18-month-old female or male animals as reference for each treatment grouped. Values were all added together and compared with paired t test. **$p < 0.001$.

(C and D) The splenocytes were harvested from the spleens of treated and control mice after 6 months of treatment (24 months old, 5 animals for each treatment per sex). Harvested

cells were stimulated in culture with PMA, ionomycin, and Brefeldin for 6 h, and IL-10 production was detected using intracellular staining. The gating strategy is shown for CD4/CD8 positive T cells in (C) female and (D) male. Summary of data plotted as bar graphs show positive IL-10 cells as percent of total CD4/CD8 T cells. Data are mean ± SEM, *$p < 0.05$, **$p < 0.01$ (two-tailed t test).

(E and F) qRT-PCR analysis of the indicated tissues of female mice.

(G–I) Ionizing radiation (IR) was used to induce senescence in IMR-90 fibroblasts *in vitro*. Cells were concurrently treated with PBS (control) or 1 mM AKG and were either mock (0 Gy) or irradiated (10 Gy). All assays were performed 10 days post irradiation.

(G) Cells were stained for senescence-associated β-galactosidase activity (left panel) or EdU incorporation (right panel).

(H) IL-6 levels in conditioned media were determined by ELISA, normalized to cell number.

(I) qRT-PCR analysis showing expression of senescence-associated secretory phenotype (SASP) genes, normalized to actin. Each dot is one independent experiment. Data are mean ± SEM, *$p < 0.05$, **$p < 0.01$ (two-tailed t test). See also Figure S6.

KEY RESOURCES TABLE

REAGENT or RESOURCE	SOURCE	IDENTIFIER
Antibodies		
Rabbit polyclonal to TRP2 (Dct)	abcam	Cat#ab74073; RRID: AB_1524517
Alexa488-conjugated donkey anti-rabbit IgG	Invitrogen	Cat#R37118; RRID: AB_2556546
Rabbit monoclonal to phosphorylated-S6 (S240/244)	Cell Signaling Technology	Cat#5364; RRID: AB_10694233
Rabbit monoclonal to phosphorylated Akt (Ser473)	Cell Signaling Technology	Cat#4058; RRID: AB_331168
Rabbit monoclonal anti S6	Cell Signaling Technology	Cat#2217; RRID: AB_331355
Rabbit monoclonal anti Akt	Cell Signaling Technology	Cat#4691; RRID: AB_915783
Rabbit monoclonal anti-GAPDH	Cell Signaling Technology	Cat#2118; RRID:AB_561053
Rabbit polyclonal to TRP2 (Dct)	abcam	Cat#ab74073; RRID: AB_1524517
Alexa488-conjugated donkey anti-rabbit IgG	Invitrogen	Cat#R37118; RRID: AB_2556546
Rabbit monoclonal to phosphorylated-S6 (S240/244)	Cell Signaling Technology	Cat#5364; RRID: AB_10694233
Rabbit monoclonal to phosphorylated Akt (Ser473)	Cell Signaling Technology	Cat#4058; RRID: AB_331168
Rabbit monoclonal anti S6	Cell Signaling Technology	Cat#2217; RRID: AB_331355
Rabbit monoclonal anti Akt	Cell Signaling Technology	Cat#4691; RRID: AB_915783
Rabbit monoclonal anti-GAPDH	Cell Signaling Technology	Cat#2118; RRID:AB_561053
Rat monoclonal anti-mouse CD4 conjugated with Brilliant Violet 650, clone GK1.5	Biolegend	Cat#100545; RRID:AB_11126142
Rat monoclonal anti-mouse CD8a conjugated with Alexa Fluor® 488, clone 53-6.7	Biolegend	Cat#100723; RRID:AB_389304
Hamster monoclonal anti-mouse TCR β chain conjugated with PerCP/Cyanine5.5, cloneH57-597	Biolegend	Cat#109228; RRID:AB_1575173
Rat monoclonal anti-mouse IL-10 conjugated with PE, clone JES5-16E3	Biolegend	Cat#505008; RRID:AB_315362
Rat monoclonal anti-mouse TNF-α conjugated with APC, clone MP6-XT22	Biolegend	Cat# 506308; RRID:AB_315429
Rat monoclonal anti-mouse Ly-6G conjugated with FITC, clone 1A8	Biolegend	Cat#127606; RRID:AB_1236494
Rat monoclonal anti-mouse CD11b conjugated with APC, clone M1/70	Biolegend	Cat#101212; RRID:AB_312795
Rat monoclonal anti-mouse CD62L conjugated with APC, clone MEL-14	Biolegend	Cat#104412; RRID:AB_313099
Rat monoclonal anti-mouse CD45 conjugated with BV510, clone 30-F11	Biolegend	Cat# 103138; RRID:AB_2563061
Rat monoclonal anti-mouse CD44 conjugated with APC-Cy7, clone IM7	Biolegend	Cat#103028; RRID:AB_830785
Rat monoclonal anti-mouse CD25 conjugated with Pacific Blue, clone PC61	Biolegend	Cat# 102022; RRID:AB_493643
Hamster monoclonal anti-mouse CD69 conjugated with Brilliant Violet 711, clone H1.2F3	Biolegend	Cat# 104537; RRID:AB_2566120
Rat monoclonal anti-mouse F4/80 conjugated with BV510, clone BM8	Biolegend	Cat#123135; RRID:AB_2562622
Hamster monoclonal anti-mouse CD11c conjugated with Pacific Blue, clone N418	Biolegend	Cat#117322; RRID:AB_755988
Rat monoclonal anti-mouse MHC Class II (I-AI/E) conjugated with APC-Cy7, clone M5/114.15.2	Biolegend	Cat#107602; RRID:AB_313317
Mouse monoclonal anti-mouse NK1.1 conjugated with BV650, clone PK136	Biolegend	Cat#108736; RRID:AB_2563159

REAGENT or RESOURCE	SOURCE	IDENTIFIER
Chemicals, Peptides, and Recombinant Proteins		
Control diet	Envigo	Teklad-2918
Calcium Alpha-Ketoglutarate Supplemented Diet (2%, 2918)	Envigo	TD.160292
Alpha-ketoglutarate Calcium	Carbosynth	71686-01-6
Phorbol 12-Myristate 13-Acetate (PMA)	Sigma	Cat#P1585
Ionomycin Calcium Salt	Sigma	Cat#I0634
Brefeldin A	Sigma	Cat# B7651
TRIzol™ Reagent	Invitrogen	Cat#15596026
5-Bromo-4-chloro-3-indolyl β-D-galactopyranoside	Sigma	Cat#B4252
Critical Commercial Assays		
Mouse cytokine/chemokine array 31-Plex	Eve technologies	MD31
Quick-RNA MiniPrep Kit	Zymo	11-328
High Capacity cDNA RT kit	R&D Systems	Cat#4368813
ProLong Antifade kit	Molecular Probes	Cat#P7481
Foxp3 / Transcription Factor Staining Buffer Set	eBioscience	Cat#00-5523-00
Click-iT™ EdU Cell Proliferation Kit for Imaging, Alexa Fluor™ 488 dye	ThermoFisher	C10337
ISOLATE II RNA mini kit	Bioline	BIO-52073
IL-6 (human) AlphaLISA Detection Kit	Perkin Elmer	AL223C
Detergent compatible (DC) protein assay kit	Bio-rad	Cat#5000112
Deposited Data		
Longitudinal Heathspan data (Female and male)	This paper; Mendeley Data	https://doi.org/10.17632/zr4ffhd3k9.1
R Codes for Statistical Data Analysis	This paper; Mendeley Data	https://doi.org/10.17632/ytstmynn4m.1
Experimental Models: Cell Lines		
Human: IMR-90 fetal lung fibroblasts	ATCC	CCL-186
Experimental Models: Organisms/Strains		
Mouse: aged C57BL/6J Female and male mice	Jackson Laboratories	JAX:000664
Oligonucleotides		
See Table S3	N/A	N/A
Software and Algorithms		
OASIS 2 software	Han et al. (2016) Oncotarget 11269	https://sbi.postech.ac.kr/oasis2/
Prism 8.1.0	GraphPad	https://www.graphpad.com/scientific-software/prism/
R Core team software version 4.0.1	R Foundation for Statistical Computing	https://cran.r-project.org
Python Software	Centrum voor Wiskunde en Informatica	https://www.python.org/downloads/
ImageJ software	Schneider et al., 2012	https://imagej.nih.gov/ij/
CalR	Mina et al., 2018	https://calrapp.org
FlowJo 10.6.1	Becton, Dickinson & Company	https://www.flowjo.com/solutions/flowjo/downloads
Other		

REAGENT or RESOURCE	SOURCE	IDENTIFIER
Promethion Metabolic Cage System	Sable Systems International	http://www.sablesys.com
31- Clinically relevant frailty phenotype	Susan E. Howlett Whitehead et al., 2014	https://doi.org/10.1093/gerona/glt136
Expedata-P Data Analysis Software	Sable Systems international	N/A